

Distinguishing ‘Higgs’ Spin Hypotheses using $\gamma\gamma$ and WW^* Decays**John Ellis^{1,2}, Ricky Fok³, Dae Sung Hwang⁴, Verónica Sanz^{2,3}, and Tevong You¹**¹*Theoretical Particle Physics and Cosmology Group, Physics Department,
King’s College London, London WC2R 2LS, UK*²*TH Division, Physics Department, CERN, CH-1211 Geneva 23, Switzerland*³*Department of Physics and Astronomy, York University, Toronto, ON, Canada M3J 1P3*⁴*Department of Physics, Sejong University, Seoul 143747, South Korea***Abstract**

The new particle X recently discovered by the ATLAS and CMS Collaborations in searches for the Higgs boson has been observed to decay into $\gamma\gamma$, ZZ^* and WW^* , but its spin and parity, J^P , remain a mystery, with $J^P = 0^+$ and 2^+ being open possibilities. We use `PYTHIA` and `Delphes` to simulate an analysis of the angular distribution of $gg \rightarrow X \rightarrow \gamma\gamma$ decays in a full 2012 data set, including realistic background levels. We show that this angular distribution should provide strong discrimination between the possibilities of spin zero and spin two with graviton-like couplings: $\sim 3\sigma$ if a conservative symmetric interpretation of the log-likelihood ratio (LLR) test statistic is used, and $\sim 6\sigma$ if a less conservative asymmetric interpretation is used. The WW and ZZ couplings of the Standard Model Higgs boson and of a 2^+ particle with graviton-like couplings are both expected to exhibit custodial symmetry. We simulate the present ATLAS and CMS search strategies for $X \rightarrow WW^*$ using `PYTHIA` and `Delphes`, and show that their efficiencies in the case of a spin-two particle with graviton-like couplings are a factor $\simeq 1.9$ smaller than in the spin-zero case. On the other hand, the ratio of $X_{2^+} \rightarrow WW^*$ and ZZ^* branching ratios is larger than that in the 0^+ case by a factor $\simeq 1.3$. We find that the current ATLAS and CMS results for $X \rightarrow WW^*$ and $X \rightarrow ZZ^*$ decays are compatible with custodial symmetry under both the spin-zero and -two hypotheses, and that the data expected to become available during 2012 are unlikely to discriminate significantly between these possibilities.

October 2012

1 Introduction and Summary

A new particle X with mass ~ 125 to 126 GeV has been discovered by the ATLAS [1] and CMS [2] Collaborations during their searches for the Higgs boson of the Standard Model. At first sight, the new particle X is observed to have similar characteristics to the long-sought Higgs particle H : it is a boson that does not have spin one, and hence it is different in character from gauge bosons. But is it really a (the) Higgs boson?

Answering this question will require a number of consistency checks. For example, are the X couplings to other particles (at least approximately) proportional to their masses? A first step towards answering this question was taken in [3] (see also [4]), where it was shown that the data published in the ATLAS and CMS discovery papers [1, 2] and other public documents, in combination with results from the TeVatron experiments CDF and D0 [5], are inconsistent with mass-independent couplings to the t, Z^0, W^\pm and b , and in fact highly consistent with linear scaling $\sim M/v$, where $v \sim 246$ GeV is the expected electroweak symmetry-breaking scale. This type of consistency check will be improved significantly with upcoming data.

However, an even more basic question is whether the recently-discovered Higgs candidate has the spin-parity $J^P = 0^+$ expected for the scalar Higgs boson in the Standard Model, and several ways to test this have been proposed. For example, some of us have recently pointed out [6] that the XV invariant mass distributions in associated production of the X particle together with a vector boson $V = Z$ or W are in theory very different for the J^P assignments $0^+, 0^-$ and 2^+ for the X particle (where we assume graviton-like couplings in the last case). We have also shown that these differences in the VX mass distributions are maintained in simulations with realistic detector cuts applied, and hence may be used to obtain indications on the J^P of the X particle, if the experimental backgrounds can be suppressed sufficiently. At the time of writing, the TeVatron experiments CDF and D0 have reported evidence for X production in association with vector bosons V , followed by $X \rightarrow \bar{b}b$ decay, at a rate compatible with the Standard Model [5], but have not yet reported the VX mass distributions. The most important backgrounds are expected to have small invariant masses. (Non-)observation of a similar VX signal in ATLAS or CMS at the Standard Model level with an invariant mass distribution corresponding to the 2^+ prediction would provide evidence for (against) the 2^+ hypothesis.

Here we first study the potential discriminating power of the angular distribution of $gg \rightarrow X \rightarrow \gamma\gamma$ events, which we simulate using PYTHIA and the Delphes, including realistic background levels. We find that the data already available may be able to offer some dis-

crimination, and that the data likely to be available to the ATLAS and CMS Collaborations by the end of 2012 should be able to distinguish between the spin-zero and graviton-like spin-two hypotheses at about the $3\text{-}\sigma$ level if a conservative symmetric interpretation of the LLR test statistic is used, or over 6σ if a less conservative asymmetric interpretation is used.

There have been many suggestions to exploit correlations among decay products of the ‘Higgs’ to identify its spin and parity [7]. Some of these correlations have been incorporated in the Higgs search strategies adopted by the ATLAS, CMS, CDF and D0 collaborations. These are based on the assumption that its $J^P = 0^+$ and have, in general, lower efficiencies for detecting a particle with different J^P . For example, the ATLAS and CMS searches for $H \rightarrow WW^* \rightarrow \ell^+\ell^-\nu\bar{\nu}$ decay make use of the kinematic correlations expected for a scalar particle, and the search by CMS for $H \rightarrow ZZ^* \rightarrow 4\ell^\pm$ also exploits the correlations expected in decays of a spin-zero particle.

We study here whether the logic can be inverted to argue that the results of these searches already favour the spin-zero hypothesis for the X particle over the spin-two hypothesis. We find that the current ATLAS and CMS measurements favour custodial symmetry for the XWW and XZZ both if the X particle has $J^P = 0^+$ and if it has $J^P = 2^+$ and graviton-like couplings. This result is based on simulations of the ATLAS and CMS $H \rightarrow WW^*$ searches using `PYTHIA` and `Delphes`, which indicate that their efficiencies are a factor $\simeq 1.9$ lower under the spin-two hypothesis. On the other hand, this effect is partially offset by the ratio of the $X \rightarrow WW^*$ and ZZ^* branching ratios that is larger by a factor $\simeq 1.3$ in the 2^+ case. Extrapolation to the full expected 2012 data set suggests that it will not be able to discriminate significantly between the 0^+ and graviton-like 2^+ hypotheses using the ratio of $X \rightarrow WW^*$ and ZZ^* decays.

2 Possible spin-parity assignments

As is well known, the fact that the new particle has been observed to decay into a pair of on-shell photons implies that it cannot have spin one [1, 2]. Accordingly, here we consider the spin-zero and spin-two options. In the spin-zero case, we consider the pseudoscalar possibility $J^P = 0^-$ as an alternative to the assignment 0^+ expected for the Standard Model Higgs boson, and we consider spin-two models with graviton-like couplings.

2.1 Pseudoscalar couplings

In this case, the following are the couplings to two vector bosons and a fermion-antifermion pair, respectively:

$$V_\mu V_\nu : \epsilon_{\mu\nu\rho\sigma} p^\rho q^\sigma, \quad \bar{f}f : \gamma_5. \quad (1)$$

where the first term corresponds to an $\epsilon_{\mu\nu\rho\sigma} F^{\mu\nu} F^{\rho\sigma} X$ interaction term, with p_μ and q_ν the sum and difference of the four-momenta of the two vector bosons, respectively. In this case, the forms of the vertices are unique, though the normalizations are arbitrary. We assume a custodial symmetry so that the pseudoscalar couplings to W^\pm and Z are equal, but make no assumptions about the ratio of the pseudoscalar couplings to the photon and gluon.

2.2 Tensor couplings

Several forms are possible for the couplings of a spin-two particle to two vector bosons. It was shown in [8] that Lorentz and Standard Model gauge symmetries forbid couplings of a massive spin-2 particle to two Standard Model particles through dimension-four terms in the Lagrangian and, assuming the flavour and CP symmetries of the Standard Model, it should couple flavour-diagonally via dimension-five terms that take the same forms as their energy-momentum tensors, namely

$$\mathcal{L}_{int} = -\frac{c_i}{M_{eff}} G^{\mu\nu} T_{\mu\nu}^i, \quad (2)$$

where the $T_{\mu\nu}^i$ are the four-dimensional stress tensors of the Standard Model species $i = b, f, V, \dots$, where V denotes a generic gauge boson. In scenarios with extra dimensions, M_{eff} is the effective Planck mass suppressing the interactions ($M_{eff} \simeq \text{O}(\text{TeV})$), whereas in composite models it denotes a scale related to confinement.

In the specific cases of vector boson fields V_μ , one has:

$$T_{\mu\nu}^V = -F_\mu^\rho F_{\rho\nu} + (\mu \leftrightarrow \nu) - m_V^2 V_\mu V_\nu, \quad (3)$$

where $F_{\mu\nu}$ is the field strength tensor for V_μ and the vector boson mass term $\propto m_V^2$ would be absent for the photon and gluon. In the case of a fermion f , one has

$$T_{\mu\nu}^f \supset \frac{i}{2} \bar{\psi} \gamma_\mu \partial_\nu \psi + (\mu \leftrightarrow \nu) + \text{h.c.} - m_f \bar{\psi} \psi g_{\mu\nu}. \quad (4)$$

Since the couplings of a composite spin-two particle and a massive graviton Standard Model particles would both take the forms (2), the model dependence would appear in the coefficients c_i . In the case of a resonance in a strong sector, these coefficients would reflect

the underlying dynamics and the quantum numbers of the constituent fields. For example, if the constituents do not carry color, the coupling to gluons, c_g , would be zero, whereas the coupling to photons, c_γ , would reflect their electric charges.

A more specific scenario is that of massive gravitons in warped extra dimensions, with the Standard Model particles residing in the bulk [9]. In five-dimensional scenarios with a factorizable metric

$$ds^2 = w^2(z)(\eta_{\mu\nu}dx^\mu dx^\nu - dz^2), \quad (5)$$

one may consider various possibilities. For example, whereas in a flat extra dimension $w(z) = 1$, in an AdS extra dimension $w(z) = z_{UV}/z$. If a Standard Model field lives on a brane located at $z_* \in (z_{UV}, z_{IR})$, one has

$$c \simeq \frac{w(z_{IR})}{w(z_*)}. \quad (6)$$

In flat extra dimensions there would be no parametric suppression, $w = 1$ and the couplings (6) would be universal¹. However, in warped extra dimensions with $w(z_{IR}) \ll w(z_{UV})$ and for a field living on the UV brane $c = w(z_{IR})/w(z_{UV}) \simeq 1 \text{ TeV}/M_P$ [10]. On the other hand, couplings to massless gauge bosons would be suppressed by the effective volume of the extra dimension, namely [11]

$$c \simeq 1 / \int_{z_{UV}}^{z_{IR}} w(z) dz. \quad (7)$$

In the AdS case, this suppression would be by $\log(z_{IR}/z_{UV}) \simeq \log(M_P/\text{TeV}) \sim 30$, whereas in flat space the suppression would be by the entire volume of the extra dimension. In either case, the couplings for gluons and photons would be equal: $c_g = c_\gamma$, assuming that localized kinetic terms are not unnaturally big.

We note that, in either case, custodial symmetry is ensured for the spin-two couplings to the massive vector bosons of the Standard Model. The reason is gauge invariance: the graviton couples to the gauge eigenstates W^a universally, which implies that $c_W = c_Z$ as $g' \rightarrow 0$. Once electroweak symmetry breaking occurs, the graviton would feel the effect through couplings like $G_{\mu\nu} D^\mu \Sigma^\dagger D^\nu \Sigma$, where Σ is a physical or spurion field, and $\langle \Sigma \rangle = v$. As Σ should respect an approximate custodial symmetry (as indicated by the small value of the T and $\Delta\rho$ parameters [12]), the spin-two particle inherits the approximate custodial symmetry.

If we assume that electroweak symmetry is broken by boundary conditions on the IR brane, we expect that the support of the W and Z wave functions will be suppressed in the

¹We note that in flat extra dimensions one typically finds conservation of a Kaluza-Klein parity that would forbid the coupling of the massive graviton to two light Standard Model particles.

neighbourhood of this brane, so that $c_{W_t, Z_t} < c_{\gamma, g}$, where the V_t are the transverse components. On the other hand, the longitudinal W and Z are localized near the IR brane [13], as the wave functions of massive fermions such as the b and t , so that $c_{W_L, Z_L}, c_{b, t} > c_{\gamma, g}$. and the wave functions of light fermions such as the u and d are expected to be concentrated closer to the UV brane, so that $c_{u, d} \ll c_{\gamma, g}$.

To summarize, in warped extra dimensions one expects the following qualitative behaviour

$$\text{Warped AdS} \quad : \quad c_b, c_t > c_W \simeq c_Z \gg c_\gamma = c_g \gg c_u, c_d. \quad (8)$$

with, e.g., $c_b \simeq 30 c_{\gamma, g}$ in the case of a Randall-Sundrum model with the third generation located near the UV brane [9, 14]. In Section 4 below, we focus on the question whether the custodial symmetry relation $c_W \simeq c_Z$ is compatible with the present experimental data.

3 Angular distributions in $X_{0,2} \rightarrow \gamma\gamma$ decay

In the case of a spin-0 particle, X_0 , its decay products are isotropically distributed over a two-dimensional sphere, so one expects a flat distribution as a function of $\cos \theta^*$, where θ^* is the angle of the photon relative to the beam axis in the X rest frame. On the other hand, the $\gamma\gamma$ angular distribution will in general be non-isotropic in the case of a spin-2 particle, X_2 . Assuming that the gluon-gluon fusion process dominates X_2 production, and graviton-like couplings of X_2 to both gluons and photons as discussed in Section 2, the $\gamma\gamma$ angular distribution in the X_2 centre of mass in gluon-gluon collisions was calculated in [15] (see also [16]), and is given by

$$\frac{d\sigma}{d\Omega} \sim \frac{1}{4} + \frac{3}{2} \cos^2 \theta^* + \frac{1}{4} \cos^4 \theta^* \quad , \quad (9)$$

which can in principle be distinguished from the isotropic distribution expected in the 0^+ and 0^- cases.

In order to see whether these theoretical distributions are distinguishable in practice, we simulated samples of spin-0 and spin-2 production accompanied by 0, 1 or 2 jets, followed by decay to two photons:

$$pp \rightarrow X_{0,2}(\rightarrow \gamma\gamma) + (0, 1, 2) \text{ jets} \quad (10)$$

using `Madgraph5` [17], which implements graviton-like couplings in the 2^+ case. Our simulation includes gluon fusion, vector boson fusion and production in association with the top

and vector bosons, in the same proportions as in the case of a conventional Higgs boson². The events are then matched using the MLM scheme in PYTHIAv6.4 [18], and passed through the Delphes [19] simulation code.

Figure 1 displays the $\cos\theta$ (left) and $\cos\theta^*$ (right) distributions after implementing the baseline cuts $p_T^\gamma > 20$ GeV and $|\eta|_\gamma < 2.5$. We see that the theoretical difference between the scalar Higgs and graviton-like 2^+ decay distributions in the rest frame of $X_{0,2}$ survives these basic cuts.

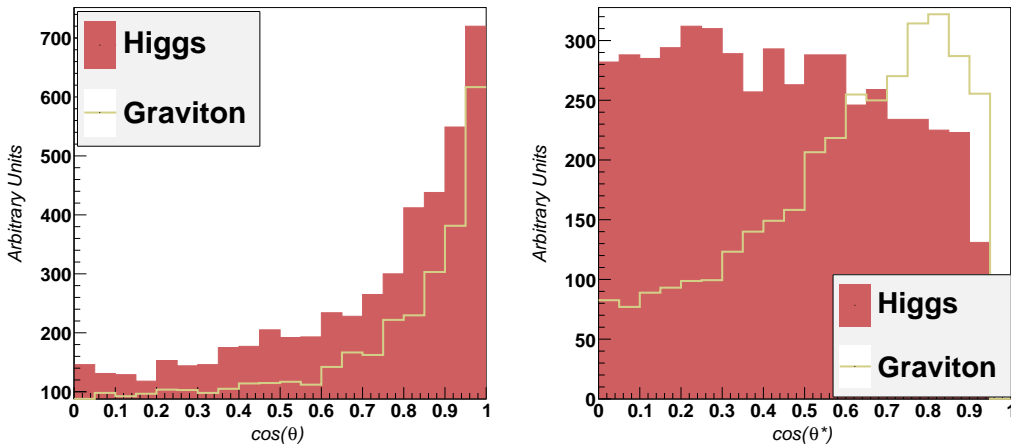


Figure 1: Simulation of the $X_{0,2} \rightarrow \gamma\gamma$ polar angle distributions obtained using MadGraph5, PYTHIAv6.4 and Delphes, after implementing the baseline cuts $p_T^\gamma > 20$ GeV and $|\eta|_\gamma < 2.5$. The left panel show distributions in the laboratory frame, and the right panel show distributions in the diphoton centre-of-mass frame.

We have studied whether the higher-level selection cuts could affect the distributions and the discriminating power between the spin-zero and -two hypotheses. As shown in Fig. 2, we find that the distinction is quite stable under changes in the photon momentum cuts, e.g., to $p_T^{\gamma_{1,2}} > 40, 25$ GeV, or in the p_{Tt} cut separating the glue-gluon and vector-boson-fusion-enhanced processes³.

3.1 Toys and Statistical Procedure

As a first step in our analysis, we use a simple angular asymmetry variable as in [20] to quantify the separation significance between spin 0^+ and 2^+ as a function of the number of

²To the extent that these other production mechanisms are suppressed relative to $gg \rightarrow X$, their inclusion or omission is not important. We have checked that their inclusion in our simulation does not affect significantly the angular distributions from $gg \rightarrow X$ alone.

³We define $p_{Tt} \equiv |\vec{p}_T^\gamma \times \vec{t}|$, where the thrust vector is defined as $\vec{t} \equiv (\vec{p}_T^{\gamma_1} - \vec{p}_T^{\gamma_2})/|\vec{p}_T^{\gamma_1} + \vec{p}_T^{\gamma_2}|$.

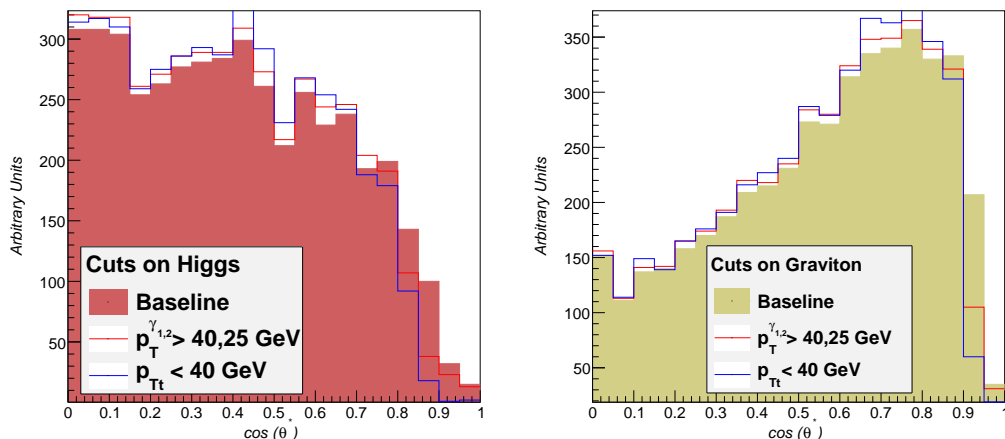


Figure 2: *The effects of different selection cuts in $p_T^{\gamma_{1,2}}$ and p_{Tt} on the angular distributions for the spin-zero case (left panel) and the graviton-like spin-two case (right panel).*

signal events in Monte-Carlo (MC) simulations, starting with the idealized case of only signal events, then showing how the asymmetry can be extracted in the presence of background and describing how this can be simulated with toy MCs. The result is presented for different signal to background (S/B) ratios representing different event sub-categories. We then repeat the analysis using the complementary log-likelihood ratio (LLR) test statistic, finding results that are somewhat more sensitive ⁴.

A reference sample of 10000 spin-zero signal diphoton events from the process $pp \rightarrow h \rightarrow \gamma\gamma$ was generated using MadGraph5 v1.4.8.3 [17] and passed through an ATLAS detector simulation based on Delphes [19]. After transforming the diphoton system to its centre-of-mass frame, baseline P_T cuts of 40 and 25 GeV were applied on the leading and sub-leading photons, respectively. As shown above, the angular distribution does not vary appreciably before and after the detector simulation and cuts. The angular distribution of this reference sample was reweighted to obtain a spin-two reference sample. These reference histograms were then sampled repeatedly to provide toy histograms with numbers of signal events that could be expected realistically. We have checked that this procedure gives results similar to generating each toy individually.

For each toy, we first quantify the shape of the distribution in $\cos\theta^*$ by an asymmetry variable, defined as

$$A = \frac{N_{\text{centre}} - N_{\text{sides}}}{N_{\text{centre}} + N_{\text{sides}}} \quad , \quad (11)$$

where N_{centre} is the number of events lying within the range $-0.5 \leq \cos\theta^* \leq 0.5$ and N_{sides}

⁴For a discussion of the relative merits of the LLR and the asymmetry variable, see [20].

is the number of events outside this range. Populating a histogram of the asymmetry value for each toy gives a distribution around different means for the spin-zero and -two toys, as illustrated in Fig. 3 for 10000 toys of 160 signal events.

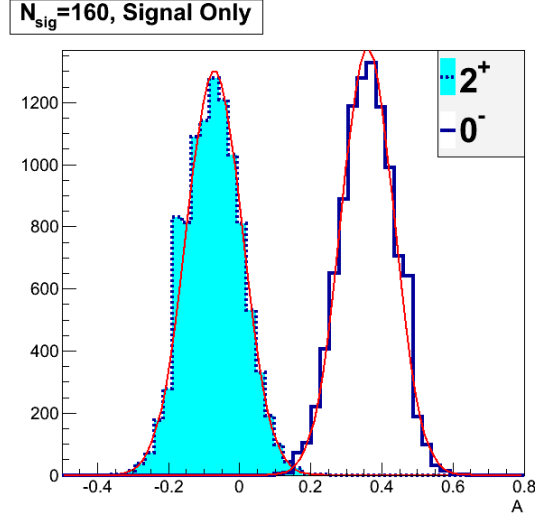


Figure 3: *Distribution of the signal angular asymmetry variable A (11) for 10000 toys of 160 signal events each, with a superimposed Gaussian fit in red. The histogram for the spin-zero toys is unshaded, and that for the spin-two toys is shaded blue. These plots do not take backgrounds into account.*

Using the asymmetry (11) as our test statistic, with a distribution that is fit well by a Gaussian (as seen in Fig. 3) to obtain a normalized probability distribution function $\text{pdf}(\Lambda)$, we quantify the separation significance using two different methods denoted as ‘asymmetric’ and ‘symmetric’.

In the *asymmetric* method one is biased towards verifying hypothesis S_1 and excluding hypothesis S_2 . Thus the value of the asymmetry that is expected to be measured by an experiment is taken to be the mean of the distribution for S_1 , namely $\Lambda_{S_1}^{\text{obs}} \equiv \Lambda_{S_1}^{\text{mean}}$, and the extent to which we can exclude hypothesis S_2 is the area β under the tail of $\text{pdf}_{S_2}(\Lambda)$:

$$\beta = \frac{\int_{-\infty}^{\Lambda_{S_1}^{\text{obs}}} \text{pdf}_{S_2}(\Lambda) d\Lambda}{\int_{-\infty}^{\infty} \text{pdf}_{S_2}(\Lambda) d\Lambda} .$$

For $\Lambda_{S_1}^{\text{mean}} > \Lambda_{S_2}^{\text{mean}}$ the integral is taken over the other side of the distribution, so as to obtain instead the area under the right tail of the distribution of S_2 . The quantity β is also known as the ‘Type II’ error, namely the probability of wrongly accepting hypothesis A in the case that actually S_2 is true.

In the *symmetric* method the two hypotheses are treated equally. One defines a $\Lambda_{\text{cut-off}}$ for which $\alpha = \beta$, namely the area α under the right tail of S_1 is equal to the area β under the left tail of S_2 (in the example where $\Lambda_{S_1}^{\text{mean}} < \Lambda_{S_2}^{\text{mean}}$). Thus, whatever the value of Λ_{obs} found by an experiment, if it lies to the left of $\Lambda_{\text{cut-off}}$ hypothesis S_1 is accepted and S_2 rejected, and vice versa if $\Lambda_{\text{obs}} > \Lambda_{\text{cut-off}}$. The significance is given by $\alpha = \beta$.

Both approaches are justified in that there is strong motivation for prioritizing the spin-zero hypothesis, and thus quoting the asymmetric significance (see also [20]). On the other hand, the symmetric approach is more objective and conservative (see [21]). In the following we quote results obtained using both methods.

The significance α is translated into n standard deviations by finding the equivalent area under a standard Gaussian distribution ⁵:

$$\alpha = \frac{1}{\sqrt{2\pi}} \int_n^\infty e^{-\frac{x^2}{2}} dx \quad . \quad (12)$$

For example, $\alpha = 0.05$ corresponds to $n = 1.64$, and the discovery standard of $n = 5$ corresponds to $\alpha = 2.87 \times 10^{-7}$.

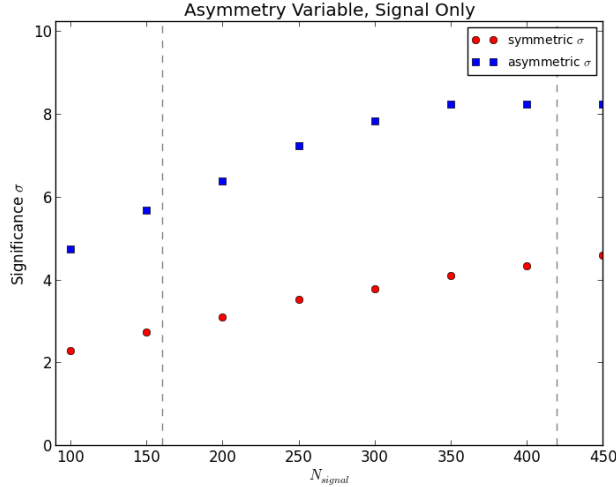


Figure 4: Numbers of standard deviations σ of separation (12) for two different methods of interpreting the statistical significance, as functions of the numbers of signal events with no background taken into account. The blue (red) dots are obtained using the asymmetric (symmetric) method, respectively. The dotted lines on the left and right are the expected yields in high and low S/B categories, respectively, with 30 fb^{-1} of integrated luminosity.

⁵This is the one-sided definition most commonly used in the literature, as opposed to the two-sided convention sometimes seen, which generally yields a higher number of standard deviations for the same p-value.

In Fig. 4 we show the separation significance defined in this way for the symmetric and asymmetric interpretations as functions of the numbers of signal events, neglecting backgrounds. The vertical dotted lines indicate the expected number of signal events in two categories that can be reached with 30 fb^{-1} of 8 TeV data collected by the end of the year. The expected yields in the two diphoton categories are obtained by combining the CMS BDT categories 0,1 and 2,3 from Table 2 of [2]. These correspond to high and low signal-to-background (S/B) ratios of approximately 0.42 and 0.19, respectively.

Note that we have not included backgrounds in Fig. 4. This figure should therefore be taken as an idealized limit of what could be achieved assuming a perfect separation of the signal from the background. In the next Section we give an estimate how the background would affect this.

3.2 Background Simulation

A reference sample of 20K QCD continuum background $pp \rightarrow \gamma\gamma$ events with the parton-level invariant masses of the diphoton pairs between 124 and 126 GeV was generated. The same detector simulation and cuts as above were applied. This sample was then used to give a number of toy background events corresponding to the desired S/B ratio.

For each toy the background and signal events are added together to give a total sample representing the available experimental information. All that can be measured is the total asymmetry in the signal region, A_{tot} . However the signal asymmetry can be extracted, since

$$\begin{aligned}
 A_{\text{tot.}} &= \frac{N_{\text{centre}} - N_{\text{sides}}}{N_{\text{centre}} + N_{\text{sides}}} \\
 &= \frac{(N_{\text{centre}}^s + N_{\text{centre}}^b) - (N_{\text{sides}}^s + N_{\text{sides}}^b)}{N_{\text{centre}}^s + N_{\text{centre}}^b + N_{\text{sides}}^s + N_{\text{sides}}^b} \\
 &= fA_s + (1 - f)A_b \quad ,
 \end{aligned} \tag{13}$$

where we assume that $f = N_s/(N_b + N_s) = (N_{\text{tot}} - N_b)/N_{\text{tot}}$ is known, and the asymmetry of the background, A_b , can in principle be measured with high accuracy in the invariant diphoton mass sideband regions outside the signal region.

The error in the experimental determination of f is the main limiting factor in reconstructing A_s . To simulate the effect of this, for each toy we randomly sample N_b from a Gaussian centered around the true value of N_b , with a one- σ width of $\sqrt{N_b}$, the statistical error. We assume that N_{tot} is measured much more accurately, so that its error can be neglected⁶. We calculate A_b using the background reference sample, so as to simulate the

⁶Adding a 1% error in N_{tot} does not affect the results.

measurement from the sidebands that is assumed to have much higher statistics.

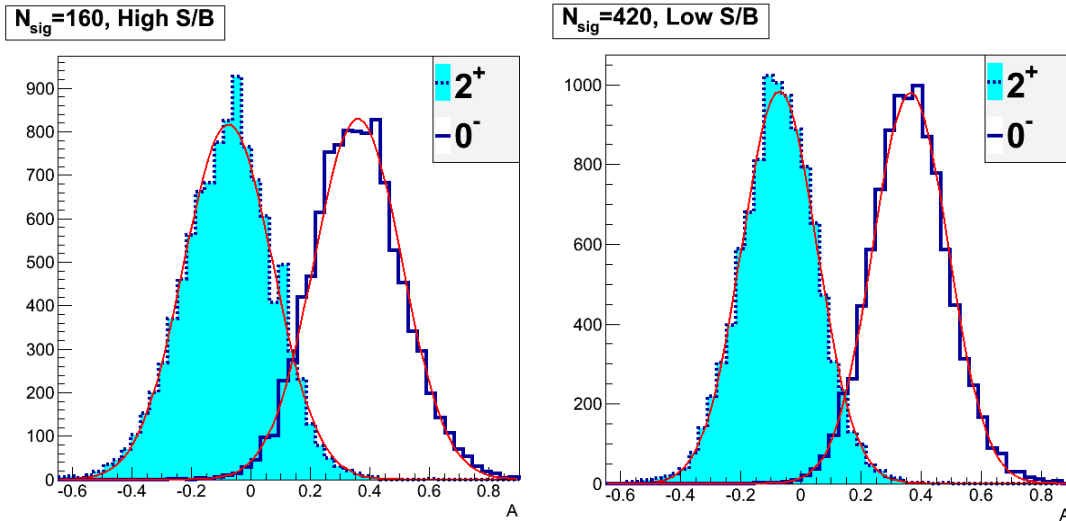


Figure 5: *Distribution of the extracted signal angular asymmetry variable A (11) for 10000 toys each. The histogram for the spin-zero toys is unshaded, and that for the spin-two toys is shaded blue. These simulations include the background with values of $S/B = 0.42$ (left) and 0.19 (right).*

As mentioned above, the benchmark luminosity that the experiments hope to attain in 2012 is 30 fb^{-1} at 8 TeV. The CMS diphoton search separates events into categories that can be approximated by two samples with high and low $S/B = 0.42$ and 0.19 , respectively, with ~ 160 and 420 expected signal events respectively for 30 fb^{-1} . The resulting distribution of A_s extracted from this simulated measurement of A_{tot} , A_b , and f per toy is illustrated in Fig. 5 for 160 signal events in the high S/B category. Fig. 6 shows the separation significance as a function of luminosity for the two categories.

We see from Fig. 6 that these simulations translate into a significance of 3 to 3.5σ in the asymmetric interpretation for each category. Ideally, a more detailed simulation should be done in which the events for each category are output from the BDT that sorts them, as this may affect the angular distribution more significantly than the simple cuts used here. As a basic check, we have verified that placing $|\eta| < 1.4$ cuts on both photons to simulate barrel-barrel events does not alter our results substantially.

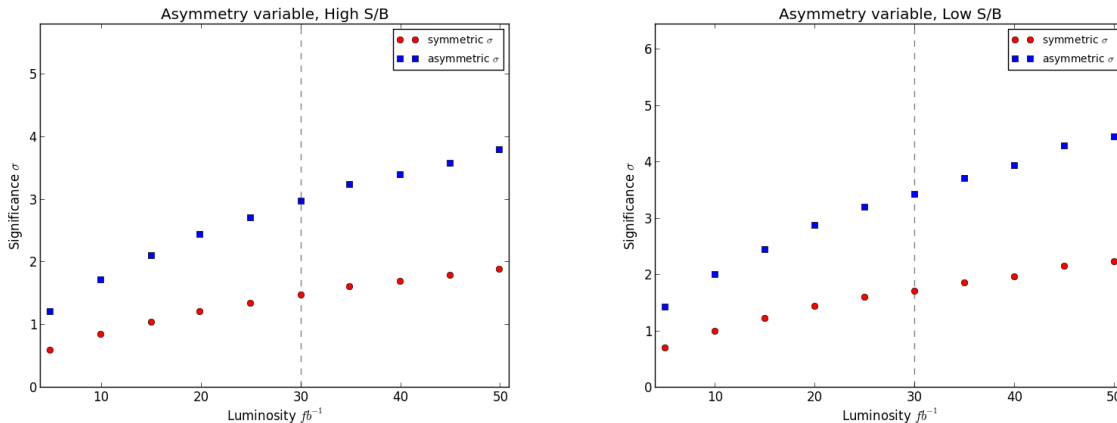


Figure 6: Numbers of standard deviations σ of separation (12) for two different methods of interpreting the statistical significance of the measurement of the angular asymmetry A , as functions of luminosity with $S/B = 0.42$ (left) and 0.19 (right). The blue (red) dots are obtained using the asymmetric (symmetric) method, respectively. Dotted lines indicate the luminosity expected by the end of 2012.

3.3 Log-Likelihood Ratio Test Statistic

An alternative test statistic is the log-likelihood ratio (LLR), for which the likelihood \mathcal{L}_S for spin hypothesis S in a single toy pseudo-experiment is defined as

$$\mathcal{L}_S = \prod_i^{\text{events}} \text{pdf}_S(x_i) \quad .$$

The probability density function in $\cos\theta^*$ of the signal is extracted from the probability to lie in a bin of the high-statistics MC from which the toys are sampled. After calculating the likelihoods for both hypothesis S_1 and S_2 we obtain the LLR for that toy by taking $-2 \ln \frac{\mathcal{L}_{S_1}}{\mathcal{L}_{S_2}}$. Thus, if we generate a set of toys for spin hypothesis S_1 (S_2), the LLR distribution will be centred around a negative (positive) mean. We may quantify the separation between these two distributions as described previously.

For a pure signal with no backgrounds, the LLR distributions for spin 0^+ and 2^+ with 160 signal events are shown in Fig. 7. Also plotted in Fig. 7 is the separation significance as a function of the number of signal events, though we emphasize that this is in idealized limit in which the signal events can be perfectly extracted from the background.

In order to include the effects of the background, we combine the background and signal MC to form a total MC, then simulate the extraction of the signal by subtracting statistically the number of background events expected in each bin from the total number of events in that bin. The number of background events per bin is smeared using a Gaussian centred on

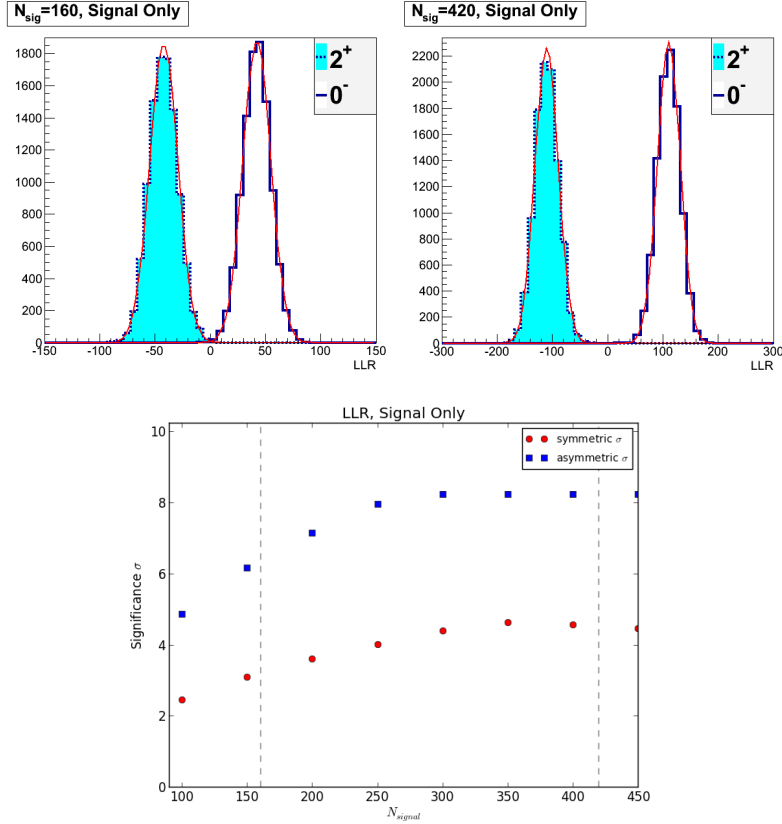


Figure 7: An example distribution of the test statistic for 160 and 420 signal events, above, and the separation significance obtained using the LLR test statistic as a function of the number of signal events, bottom. Note that no backgrounds are included here.

the true value, with a one- σ width given by the statistical error $\sqrt{N_{\text{bkg}}^{\text{bin}}}$. If the randomly smeared number of background events exceeds the total number of events in that bin the corresponding bin of the measured signal histogram is set to zero (since it cannot be negative).

Distributions in LLR and separation significance plots similar to those in Fig. 7 are shown in Fig. 8, with the backgrounds now taken into account, for both high and low values of $S/B = 0.42$ and 0.19 , respectively. We see that the high (low) S/B category for 30 fb^{-1} of 8 TeV data, corresponding to 160 (420) signal events, yields a separation significance around 3.5 (4.2) σ using the asymmetric method. A combination of the high and low categories can achieve over $6\text{-}\sigma$ separation using the asymmetric method, as is seen in Fig. 9, and $\sim 3\sigma$ using the symmetric method.

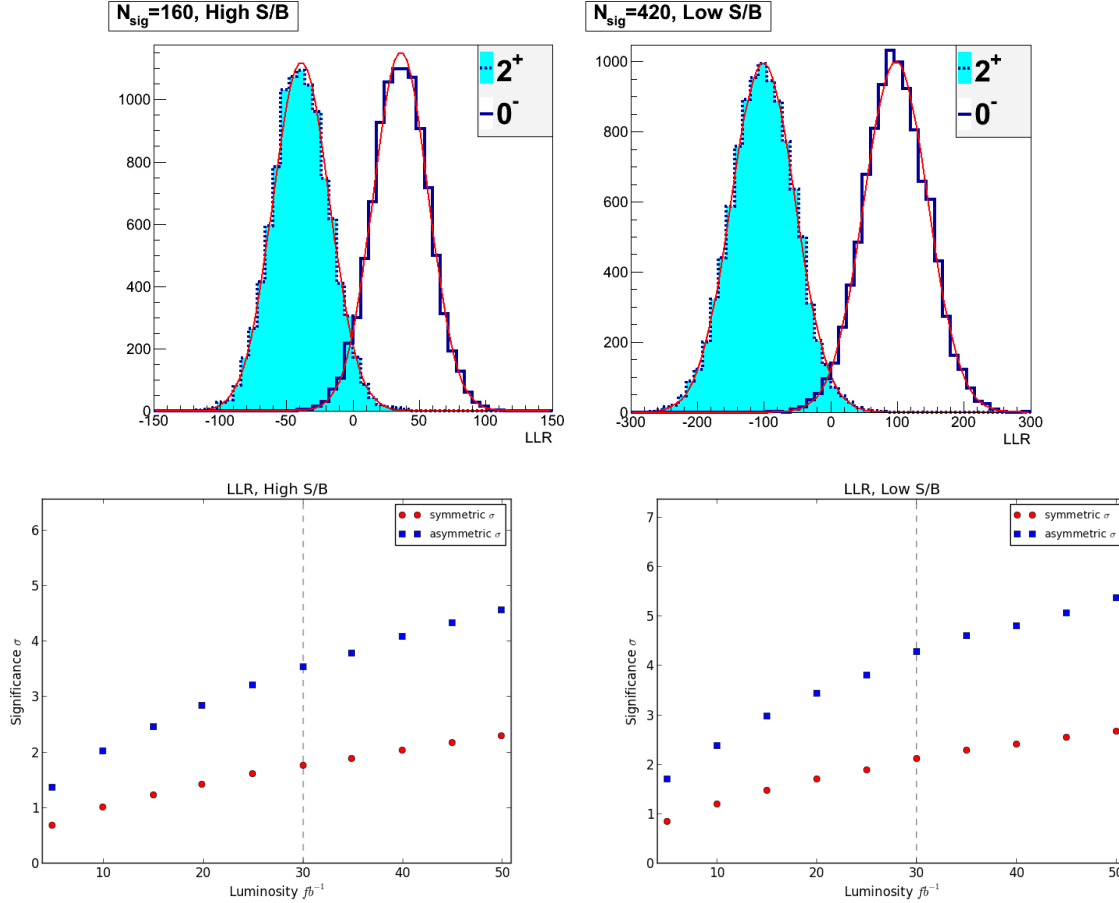


Figure 8: Separation significance using the LLR test statistic as a function of the luminosity (lower panel) and an example distribution of the test statistic for the 160 and 420 signal events expected in the high- and low-S/B categories at 30 fb^{-1} (upper panels). The backgrounds are included, with $S/B = 0.42$ (left) and 0.19 (right), respectively.

4 Angular, mass and m_T Distributions in $X_{0,2} \rightarrow WW^* \rightarrow \ell^+ \nu_\ell \ell^- \bar{\nu}_\ell$ Decay

As discussed in [16], the lepton momentum distributions and correlations are very different for the $X_{0,2}$ hypotheses. In the spin-zero case, the spins of the W^\pm and $W^{\mp*}$ must be *antiparallel*, implying that the charged leptons ℓ^\pm produced in their decays appear preferentially in the *same* hemisphere. On the other hand, in the spin-two case, the spins of the W^\pm and $W^{\mp*}$ must be *parallel*, implying that their daughter ℓ^\pm appear preferentially in the *opposite* hemisphere. As pointed out in [16], these differences in the decay kinematics imply that the dilepton invariant mass $m_{\ell\ell}$ is generally *smaller* in X_0 decay than in X_2 decay, as is the difference $\phi_{\ell\ell}$ between the ℓ^\pm azimuthal angles. A corollary is that the net transverse momenta

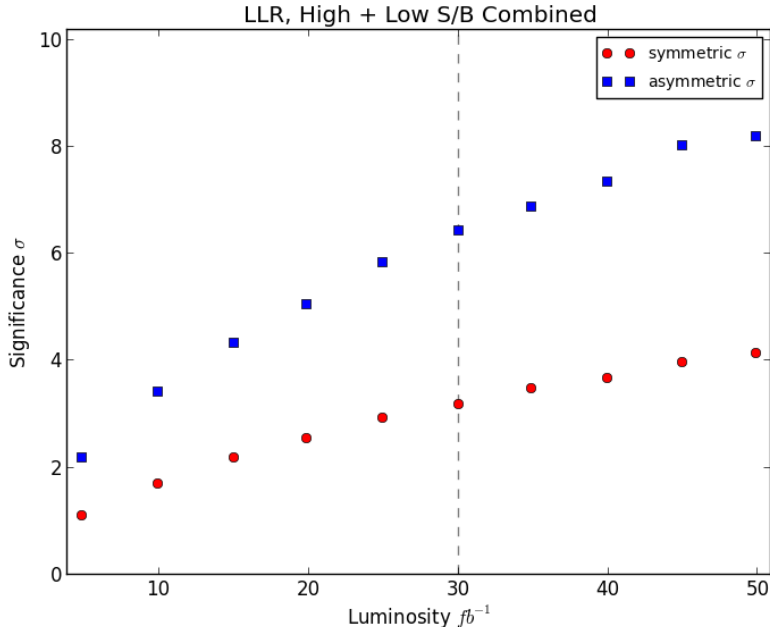


Figure 9: *Separation significance using the LLR test statistic as a function of luminosity for the combination of high- and low-S/B categories. The dotted line indicates the expected reach by the end of 2012.*

of the $\ell^+\ell^-$ pair, $p_T^{\ell_1, \ell_2}$, is generally *larger* in X_0 decay than in X_2 decay. We now address the question whether and to what extent these differences survive the event selections and cuts made by ATLAS and CMS.

Regarding the simulation details, we created new models in `Feynrules` [22], including the pseudoscalar and graviton-like spin-two couplings described in Section 2. We then interfaced with `MadGraph5` [17] using the `UFO` model format [23]. We incorporate hadronization and showering effects using `PYTHIA` [18], and detector effects using `Delphes` [19].

4.1 Simulation of ATLAS and CMS event selections

We start by implementing the baseline cuts of the ATLAS and CMS analyses: two isolated leptons ($= e, \mu$) of $p_T > 15$ GeV and $|\eta| < 2.5$. As seen in Fig. 10, the distributions in the dilepton invariant mass $m_{\ell\ell}$ (left) and in the relative azimuthal angle $\phi_{\ell\ell}$ (right) are very different in the baseline X_0 and X_2 simulations. These differences reflect the kinematical effects noted earlier. In particular, $m_{\ell\ell}$ is generally smaller in the X_0 case than in the X_2 case, as seen in Fig. 7 of [16], as is $\phi_{\ell\ell}$, reflecting the angular distribution shown in Fig. 6 of [16].

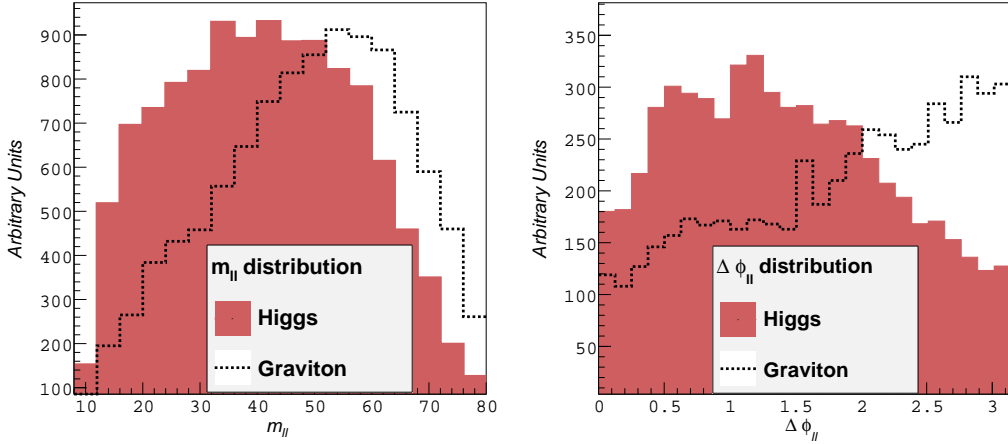


Figure 10: Results from simulations of the $X_{0+,2+} \rightarrow WW^* \rightarrow \ell^+ \nu_\ell \ell^- \bar{\nu}_\ell$ signals, using `PYTHIA` and `Delphes` and the baseline cuts described in the text. The left (right) panel displays the $m_{\ell\ell}$ ($\phi_{\ell\ell}$) distributions.

Our next step is to simulate the ATLAS search for $X \rightarrow WW^* \rightarrow \ell^+ \nu_\ell \ell^- \bar{\nu}_\ell$ events. This is based on a selection of events with two opposite-sign, unlike-flavour leptons with $p_T^{\ell_1, \ell_2} > 25, 15$ GeV in the central region, and invariant mass $m_{\ell\ell} \in [10, 80]$ GeV⁷. The events are then separated into categories with 0, 1 and 2 anti- k_T jets (defined by cones $R = 0.4$) and $p_T > 25, 30$ GeV in the central and forward regions, respectively. In the 0- and 1-jet samples used here, the dilepton invariant mass upper bound is tightened to 50 GeV. The following set of cuts is then applied to the 0-jet sample:

$$E_{T,rel}^{miss} > 25 \text{ GeV}, p_T^{\ell\ell} > 30 \text{ GeV}, \text{ and } |\Delta\phi_{\ell\ell}| < 1.8, \quad (14)$$

where $E_T^{rel} \equiv \cancel{E}_T \sin \Delta\phi_{min}$ with $\Delta\phi_{min} \equiv \min(\Delta\phi, \pi/2)$ and $\Delta\phi$ the minimum angle between the missing-energy vector and the leading lepton, the subleading lepton or any jet with $p_T > 25$ GeV. In the 1- and 2-jet case, there is an extra cut

$$|\vec{p}_T^{tot}| = |\vec{p}_T^{\ell\ell} + \vec{p}_T^j + \vec{E}_T^{miss}| < 30 \text{ GeV} \quad (15)$$

as well as a b -tag veto. In the 2-jet case we also implemented the vector-boson-fusion cuts

$$m_{jj} > 500 \text{ GeV and } |\Delta y_{jj}| > 3.8. \quad (16)$$

Finally, a cut $m_T \equiv \sqrt{(E_T^{\ell\ell} + \cancel{E}_T)^2 - |\vec{p}_T^{\ell\ell} + \vec{\cancel{p}}_T|^2} \in [93.75, 125]$ GeV is applied to emulate the fit to the distribution performed in the ATLAS analysis.

⁷We implement the relevant quality and isolation criteria at the level of the `Delphes` simulation.

Fig. 11 displays the $m_{\ell\ell}$ (upper panels) and $\phi_{\ell\ell}$ (lower panels) distributions for $X_{0+,0-}$ (left and centre panels) and X_2 (right panels) after implementing in `Delphes` the ATLAS analysis cuts described above. We see that the effect of cuts is dramatic, reshaping the distributions in the X_2 case so that it resembles the X_0 hypothesis. This is not only a consequence of the $\Delta\phi_{\ell\ell}$ cut. We have verified that one could loosen or even remove the $\Delta\phi_{\ell\ell}$ cut: its effect on the background rejection is very mild, and dropping it would not help to maintain the distinctive kinematic features of $X_2 \rightarrow WW^* \rightarrow \ell^+\nu_\ell\ell^-\bar{\nu}_\ell$ decay. The initial $p_T^{\ell\ell}$ cut plays a key role in reducing features due to the anti-parallel preference of the lepton momenta in Fig. 11, due in turn to the strong correlations between the $\Delta\phi_{\ell\ell}$, $m_{\ell\ell}$ and $p_T^{\ell\ell}$ cuts.

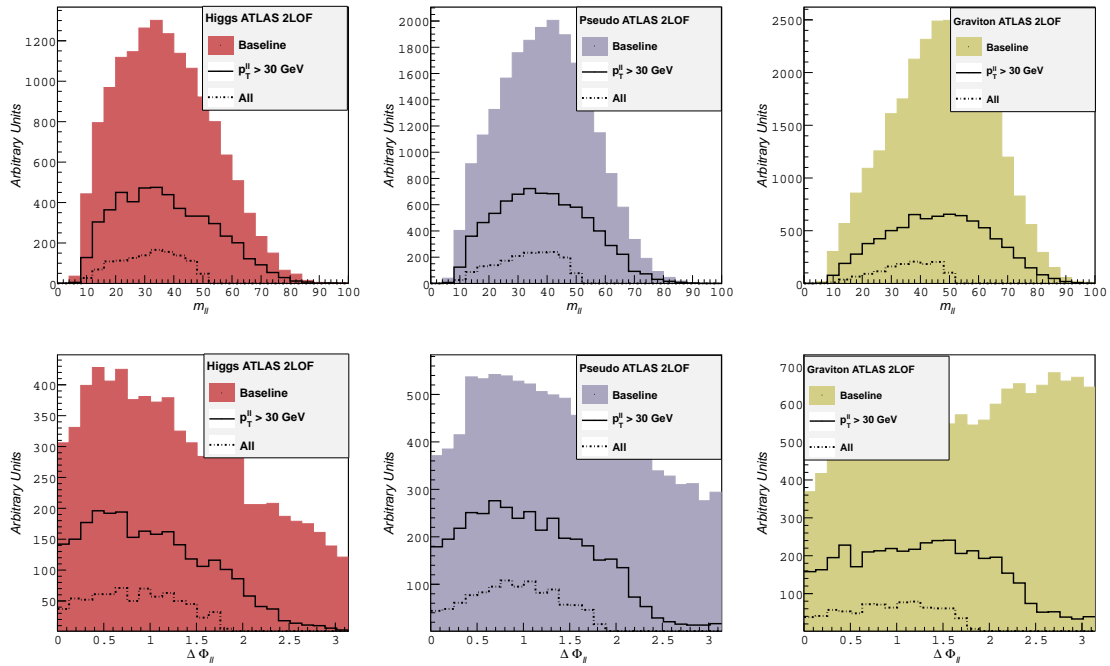


Figure 11: Results from simulations of the $X_{0+,0-,2+} \rightarrow WW^* \rightarrow \ell^+\nu_\ell\ell^-\bar{\nu}_\ell$ signals, using `PYTHIA` and `Delphes` and implementing the ATLAS cuts described in the text. The upper (lower) panels display the $m_{\ell\ell}$ ($\phi_{\ell\ell}$) distributions for $X_{0+,0-}$ (left and centre) and X_{2+} (right).

In Fig. 12, we show the m_T distributions found after implementing all the ATLAS cuts described above, under the $X_{0+,0-}$ and graviton-like X_{2+} hypotheses. They exhibit somewhat different behaviours within the selected kinematic range. The peaking of the X_{2+} histogram at slightly lower m_T than those for $X_{0+,0-}$ is a relic of the differences in the kinematic distributions before the cuts. Since the neutrino and antineutrino are emitted antiparallel in X_{2+} case, the $\bar{\nu}\nu$ invariant mass has a slight tendency to be larger than in the $X_{0+,0-}$ cases, implying that m_T tends to fall further below the X mass of ~ 125 GeV.

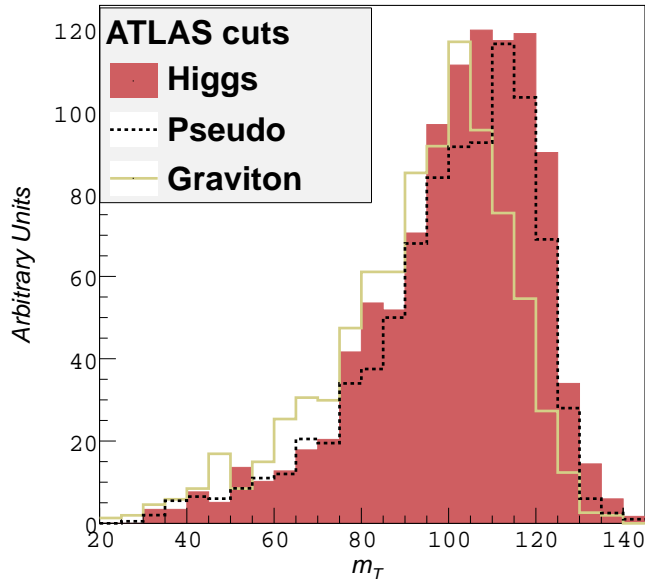


Figure 12: *The transverse mass, m_T , distribution after application of all the ATLAS cuts described in the text, under the three J^P hypotheses.*

We have also simulated the corresponding CMS search for $X_{0,2} \rightarrow WW^* \rightarrow \ell^+ \nu_\ell \ell^- \bar{\nu}_\ell$. The CMS cuts are very similar to those applied by ATLAS, except that CMS requires $p_T^{\ell\ell} > 45$ GeV, $m_{\ell\ell} \in [12, 45]$ GeV, $\Delta\Phi_{\ell\ell} < 1.6$ and $m_T \in [80, 125]$ GeV. The resulting histograms of $m_{\ell\ell}$ and $\phi_{\ell\ell}$ are very similar to those for ATLAS shown in Fig. 11, so we do not show the CMS equivalents.

We display in Table 1 the ATLAS and CMS cut flows for the different X_{J^P} hypotheses. These results are based on simulations of 10,000 0^+ events, 20,000 0^- events and 30,000 2^+ events, so the statistical errors are negligible. Although there are differences between the numbers of events surviving different stages in the ATLAS and CMS selection, the end results after applying all the cuts are very similar. Specifically, we find that the efficiencies for the 0^+ hypothesis are larger than those for the 2^+ hypothesis by factors of 1.86 (1.94) for the ATLAS (CMS) event selections, with the efficiencies for a pseudoscalar X_{0^-} being about 10% lower than that for X_{0^+} in both cases.

4.2 Data analysis under different J^P hypotheses

We now discuss how this efficiency difference in the experimental selection cuts may in principle be used to help discriminate between the scalar and graviton-like spin two hypotheses, analyze the sensitivity offered by the current data and estimate the likely sensitivity of the

Cuts	Scalar 0^+	Pseudoscalar 0^-	Graviton-like 2^+
$p_T^{\ell\ell} > 30$ (45) GeV	86 (63)	83 (58)	70 (43)
$m^{\ell\ell} < 50$ (45) GeV	66 (49)	62 (44)	40 (26)
$\Delta\Phi_{\ell\ell} < 1.8$ (1.6)	63 (49)	60 (44)	38 (26)
$m_T \in [93.75, 125]([80, 125])$ GeV	44 (40)	41 (36)	22 (21)

Table 1: *The cutflow evolutions for the ATLAS (CMS) cuts under the three J^P hypotheses. The numbers shown are the cumulative efficiencies to pass the cuts (in percent).*

full 2012 data set.

We parametrize the rescaling of X_{0+} particle couplings to the W, Z gauge bosons relative to the Standard Model values by a_W and a_Z , respectively, and infer $\lambda_{WZ} \equiv a_W/a_Z$ from the measured ratio of the signals in the WW^* and ZZ^* channels, which is given by

$$R_{WZ} = \frac{N_W}{N_Z} = \frac{BR_{SM}(X_{0+} \rightarrow WW^*)}{BR_{SM}(X_{0+} \rightarrow ZZ^*)} \left(\frac{a_W}{a_Z}\right)^2 \left(\frac{\epsilon_W}{\epsilon_Z}\right), \quad (17)$$

where $\epsilon_{W,Z}$ are the efficiencies for the $X_{0+} \rightarrow WW^*, ZZ^*$ experimental selections. Likewise, rescaling by a_{W_2} and a_{Z_2} the W and Z couplings of an X_{2+} particle relative to reference values with custodial symmetry, one has in an obvious notation

$$R_{WZ_2} = \frac{N_W}{N_Z} = \frac{BR_{2+}(X_{2+} \rightarrow WW^*)}{BR_{2+}(X_{2+} \rightarrow ZZ^*)} \left(\frac{a_{W_2}}{a_{Z_2}}\right)^2 \left(\frac{\epsilon_{W_2}}{\epsilon_{Z_2}}\right), \quad (18)$$

which can be used to infer $\lambda_{WZ_2} \equiv a_{W_2}/a_{Z_2}$ in the same way. Since we use $X \rightarrow ZZ^* \rightarrow 4\ell^\pm$ event selections that use only the individual ℓ^\pm momenta (specifically, we do not use the CMS MELA analysis), we may assume that $\epsilon_{Z_2}/\epsilon_Z = 1$. The value of λ_{WZ_2} inferred from the data therefore differs from that of λ_{WZ} by the following factor

$$\lambda_{WZ_2} = \lambda_{WZ} \times \sqrt{\left(\frac{\epsilon_W}{\epsilon_{W_2}}\right) \left(\frac{BR_{SM}(X_{0+} \rightarrow WW^*)}{BR_{SM}(X_{0+} \rightarrow ZZ^*)} / \frac{BR_{2+}(X_{2+} \rightarrow WW^*)}{BR_{2+}(X_{2+} \rightarrow ZZ^*)}\right)}, \quad (19)$$

where the value $\epsilon_W/\epsilon_{W_2} \simeq 1.9$ was calculated in the previous Section.

The ratio of the ratio of $X_{0+,2+} \rightarrow WW^*$ and ZZ^* branching ratios is not simply unity, because of the non-trivial dependences of the partial decay widths $\Gamma(X_{0+,2+} \rightarrow VV^*)$ on the masses of the vector bosons V . We have used `Madgraph5 v1.4` and `v1.5` to calculate the decay widths, and have checked our results against the Standard Model predictions for $H \rightarrow WW^*$ and ZZ^* , and also tested them in the limiting cases of heavy graviton and Higgs, when the vector bosons are produced on-shell. In the case of the physical X mass, we find

$$\frac{BR_{2+}(X_{2+} \rightarrow WW^*)}{BR_{2+}(X_{2+} \rightarrow ZZ^*)} / \frac{BR_{SM}(X_{0+} \rightarrow WW^*)}{BR_{SM}(X_{0+} \rightarrow ZZ^*)} = 1.3, \quad (20)$$

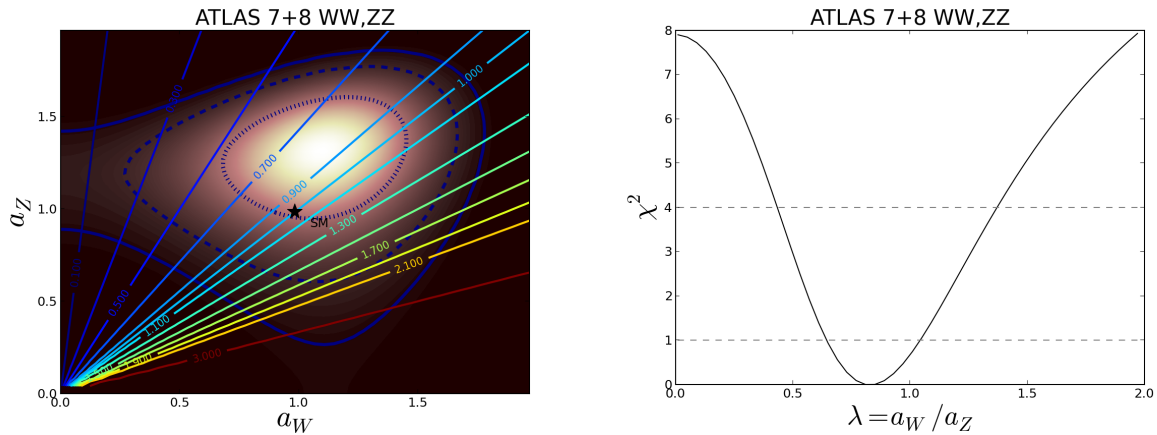


Figure 13: *Left: The (a_W, a_Z) plane displaying the 68 and 95 % CL contours (broken black and solid blue, respectively) obtained from a fit to the ATLAS 7 and 8 TeV data, with rays corresponding to contours of a_W/a_Z : the Standard Model point $a_W = a_Z = 1$ is indicated by a black star. Right: The $\Delta\chi^2$ function relative to the best-fit value in our ATLAS fit, marginalized over the magnitudes of $a_{W,Z}$, with dashed horizontal lines at $\Delta\chi^2 = 1, 4$.*

and hence

$$\lambda_{WZ_2} = \lambda_{WZ} \times 1.2, \quad (21)$$

when a_W and a_Z , and hence λ_{WZ} and λ_{WZ_2} , are extracted using only the $X \rightarrow WW^*$ and ZZ^* inclusive search channels.

In Fig. 13 we display in the left panel the (a_W, a_Z) plane with the two-dimensional CL contours that we find in our analysis of the ATLAS 7 and 8 TeV data combined⁸ [3]. Also shown to guide the eye, in this and subsequent similar plots, are rays corresponding to various values of the ratio a_W/a_Z . The ray $a_W/a_Z = 1$ passes through the Standard Model point $a_W = a_Z = 1$, which is indicated by a black star. This point also lies just within the 68% CL contour, shown as a broken black line (the 95% CL contour is a solid blue line). The right panel of Fig. 13 displays the $\Delta\chi^2$ function relative to the best-fit value in our analysis of the ATLAS 7 and 8 TeV data, marginalized over the magnitudes of $a_{W,Z}$. The combined ATLAS data do not exhibit any strong preference between the $J^P = 0^+$ and 2^+ hypotheses, which correspond to $a_W/a_Z = 1$ and $1/\sqrt{2}$, respectively.

Fig. 14 displays a similar pair of panels for our analysis of the available CMS 7 and 8 TeV data. We note here that we do not use the final CMS result for $X \rightarrow WW^*$ signal, which include an MELA selection that we do not model. Instead, we use the expected signal, background and observed event numbers shown in Table 3 of [2], which correspond directly

⁸We cannot use for this purpose the value of λ_{WZ} quoted in [24], because this incorporates information from a combination of channels including $X \rightarrow \gamma\gamma$, which supplies information on a_W that does not apply to the spin-two case.

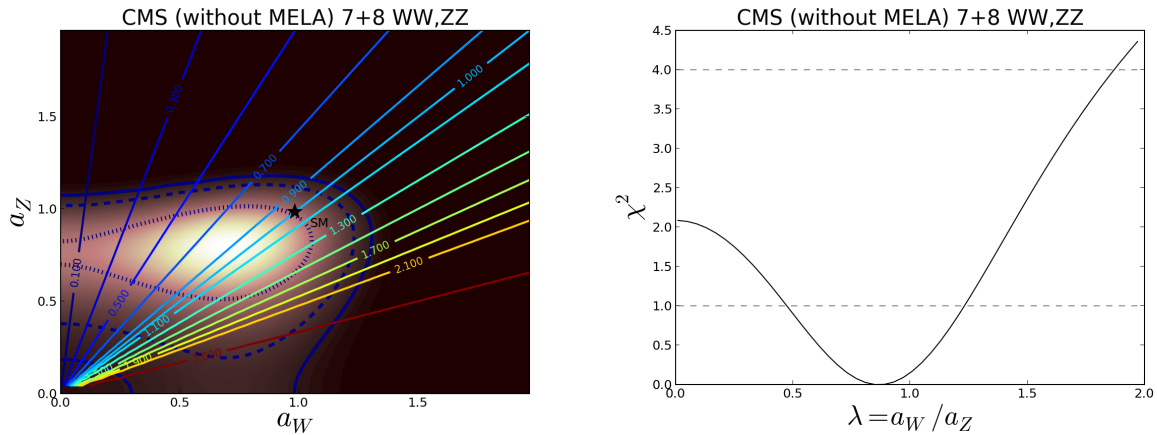


Figure 14: As in Fig. 13, but based on our fit to the CMS 7 and 8 TeV data, which does not include the final MELA selection made in [2].

to the CMS event selection and efficiency found in our simulation above. As in the ATLAS case above, the CMS data also do not exhibit a strong preference between the $J^P = 0^+$ and 2^+ hypotheses.

Fig. 15 displays a similar pair of panels for our combined analysis of the available ATLAS and CMS 7 and 8 TeV data. The data sets in combination provide no significant discrimination between the $J^P = 0^+$ and 2^+ hypotheses. Our combined χ^2 analysis yields

$$\lambda_{WZ} \equiv \frac{a_W}{a_Z} = 0.93_{-0.20}^{+0.24}. \quad (22)$$

Using (21), the corresponding value in the X_{2^+} case is

$$\lambda_{WZ_2} = 1.12_{-0.24}^{+0.29}, \quad (23)$$

and we see that both results are compatible with unity.

This result is based on $\sim 5/\text{fb}$ of data at each of 7 and 8 TeV analyzed by each of ATLAS and CMS. At the time of writing, each experiment has now recorded $\sim 15/\text{fb}$ of data at 8 TeV, corresponding approximately to a doubling of the statistics and potentially to a reduction in the uncertainty in a_W/a_Z by a factor ~ 1.4 . It is anticipated that each experiment might record $\sim 30/\text{fb}$ of data by the end of 2012, corresponding to reductions in the statistical errors in (22, 23) by factors $\sim \sqrt{3}$. If the central value remained the same, (23) would become $\lambda_{WZ_2} = 1.12_{-0.14}^{+0.17}$, whereas if the central value were to correspond to $\lambda_{WZ} = 1$, one would have $\lambda_{WZ_2} = 1.21_{-0.14}^{+0.17}$. We conclude that the best one could reasonably hope for with the 2012 data would be a deviation from the custodial symmetry prediction $\lambda_{WZ_2} = 1$ of about one σ .

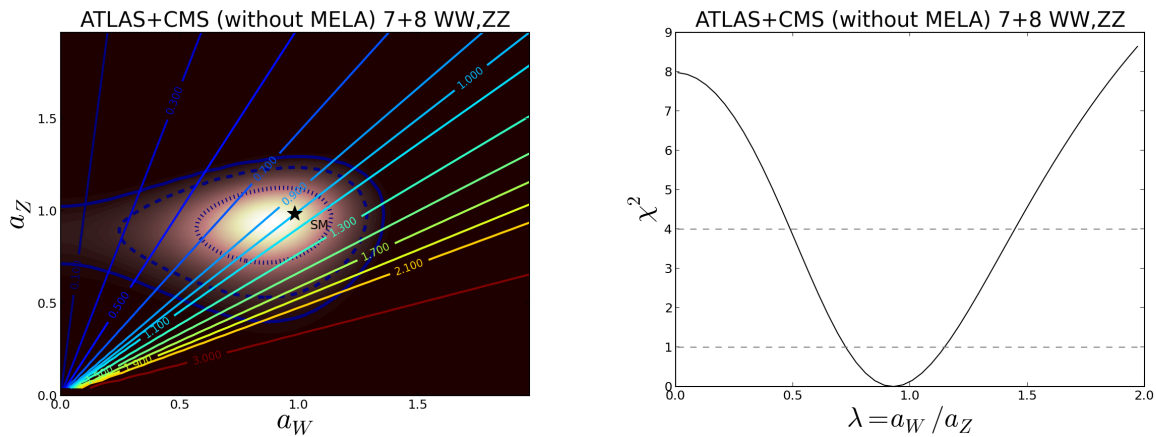


Figure 15: As in Fig. 13, but based on our combined fit to the ATLAS and CMS 7 and 8 TeV data.

5 Overview and Prospects

We have explored in this paper two strategies to help determine the spin of the new particle X discovered recently by the ATLAS and CMS Collaborations. One of these exploits the angular distribution of the final-state photons in $gg \rightarrow X \rightarrow \gamma\gamma$ decay, and the other exploits the angular distributions and correlations in $X \rightarrow WW^* \rightarrow \ell^+\ell^-\nu\bar{\nu}$ decay, which are in principle quite different for different spin assignments $J^P = 0^+, 0^-$ and 2^+ for the X particle.

We have shown how the 2012 LHC data could be used to study the angular distribution in $gg \rightarrow X \rightarrow \gamma\gamma$ decay and provide potentially significant discrimination between the spin-zero and spin-two hypotheses. A simple angular asymmetry measurement gives a discrimination power approaching that possible with a full LLR analysis. We include the effects of backgrounds in samples with both high and low $S/B = 0.42$ and 0.19 , corresponding in spirit to CMS event categories. We find that the present data should already provide some discrimination between the $J^P = 0^\pm$ and 2^+ hypotheses, and that an analysis of the full 2012 data set could provide a separation significance of $\sim 3\sigma$ if a conservative symmetric interpretation of the LLR statistic is used, rising to above 6σ if a less conservative asymmetric interpretation is used.

We have analyzed the sensitivities of the published results of the ATLAS and CMS searches for $H \rightarrow WW^*$ to the spin-parity of the X particle. Simulating these searches using PYTHIA and Delphes, we have shown that the ATLAS and CMS experimental selections

suppress the kinematic differences between 0^+ and 2^+ decays. Therefore, an analysis based on kinematic shapes would be rather inconclusive based in the published cuts.

One could hope for retaining some of the kinematic differences by changing the cuts, but those changes are limited by the need to suppress the large Standard Model WW background. A more hopeful strategy, and the one we developed in this paper, is to use of the approximate custodial symmetry in both spin-zero and -two hypothesis, to relate the WW^* and ZZ^* channels. In WW^* , the efficiencies of the searches differ by a factor $\simeq 1.9$ for X_{0^+} and X_{2^+} . On the other hand, we find that the ratio of $X_{2^+} \rightarrow WW^*$ and ZZ^* branching ratios is $\simeq 1.3$ larger than the corresponding ratio of branching ratios in the 0^+ case. The current measurements by ATLAS and CMS of the ratio of experimental rates for $X \rightarrow WW^* \rightarrow \ell^+\ell^-\nu\bar{\nu}$ and $X \rightarrow ZZ^* \rightarrow 4\ell^\pm$ are compatible with custodial symmetry in both the 0^+ and 2^+ cases, and we do not expect that this will improve significantly with the full 2012 set of LHC data.

Many other strategies to discriminate between different spin-parity hypotheses for the X particle have been proposed, including kinematic correlations in $X \rightarrow ZZ^* \rightarrow 4\ell^\pm$ decay and the threshold behaviour of associated $W/Z + X$ production, as discussed in the Introduction. We have every confidence that the spin-parity of the X particle will be pinned down within a few months, in good time for the nominations for the 2013 Nobel Physics Prize.

Acknowledgements

We thank Oliver Buchmüller, Ben Gripaios, Rakhi Mahbubani, Eduard Massó and Pierre Savard for valuable discussions. The work of JE was supported partly by the London Centre for Terauniverse Studies (LCTS), using funding from the European Research Council via the Advanced Investigator Grant 267352. The work of DSH was supported partly by the Korea Foundation for International Cooperation of Science & Technology (KICOS) and the Basic Science Research Programme of the National Research Foundation of Korea (2012-0002959). The work of TY was supported by a Graduate Teaching Assistantship from King's College London. JE, DSH and VS thank CERN for kind hospitality, and TY thanks Prof. T. Kobayashi and the Bilateral International Exchange Program of Kyoto University for kind hospitality.

References

- [1] G. Aad *et al.* [ATLAS Collaboration], Phys. Lett. B **716** (2012) 1 [arXiv:1207.7214 [hep-ex]]; see also F. Gianotti, talk on behalf of the ATLAS Collaboration at CERN, 4th July, 2012, <https://cms-docdb.cern.ch/cgi-bin/PublicDocDB//ShowDocument?docid=6126>.
- [2] S. Chatrchyan *et al.* [CMS Collaboration], Phys. Lett. B **716** (2012) 30 [arXiv:1207.7235 [hep-ex]]; see also J. Incandela, talk on behalf of the CMS Collaboration at CERN, 4th July, 2012, <https://cms-docdb.cern.ch/cgi-bin/PublicDocDB//ShowDocument?docid=6125>.
- [3] J. Ellis and T. You, JHEP **1209**, 123 (2012) [arXiv:1207.1693 [hep-ph]].
- [4] For other analyses of the X particle couplings, see also: D. Carmi, A. Falkowski, E. Kuflik and T. Volanski, arXiv:1202.3144 [hep-ph]; A. Azatov, R. Contino and J. Galloway, JHEP **1204** (2012) 127 [hep-ph/1202.3415]. J.R. Espinosa, C. Grojean, M. Muhlleitner and M. Trott, arXiv:1202.3697 [hep-ph]; P. P. Giardino, K. Kannike, M. Raidal and A. Strumia, arXiv:1203.4254 [hep-ph]; T. Li, X. Wan, Y. Wang and S. Zhu, arXiv:1203.5083 [hep-ph]; M. Rauch, arXiv:1203.6826 [hep-ph]; J. Ellis and T. You, JHEP **1206** (2012) 140, [arXiv:1204.0464 [hep-ph]]; A. Azatov, R. Contino, D. Del Re, J. Galloway, M. Grassi and S. Rahatlou, arXiv:1204.4817 [hep-ph]; M. Klute, R. Lafaye, T. Plehn, M. Rauch and D. Zerwas, arXiv:1205.2699 [hep-ph]; J.R. Espinosa, M. Muhlleitner, C. Grojean and M. Trott, arXiv:1205.6790 [hep-ph]; D. Carmi, A. Falkowski, E. Kuflik and T. Volansky, arXiv:1206.4201 [hep-ph]; M. J. Dolan, C. Englert and M. Spannowsky, arXiv:1206.5001 [hep-ph]; J. Chang, K. Cheung, P. Tseng and T. Yuan, arXiv:1206.5853 [hep-ph]; S. Chang, C. A. Newby, N. Raj and C. Wanotayaroj, arXiv:1207.0493 [hep-ph]; I. Low, J. Lykken and G. Shaughnessy, arXiv:1207.1093 [hep-ph]; T. Corbett, O. J. P. Eboli, J. Gonzalez-Fraile and M. C. Gonzalez-Garcia, arXiv:1207.1344 [hep-ph]; P. P. Giardino, K. Kannike, M. Raidal and A. Strumia, arXiv:1207.1347 [hep-ph]; M. Montull and F. Riva, arXiv:1207.1716 [hep-ph]; J. R. Espinosa, C. Grojean, M. Muhlleitner and M. Trott, arXiv:1207.1717 [hep-ph]; D. Carmi, A. Falkowski, E. Kuflik, T. Volansky and J. Zupan, arXiv:1207.1718 [hep-ph]; S. Banerjee, S. Mukhopadhyay and B. Mukhopadhyaya, JHEP **10** (2012) 062, [arXiv:1207.3588 [hep-ph]]; F. Bonner, T. Ota, M. Rauch and W. Winter, arXiv:1207.4599 [hep-ph]; T. Plehn and M. Rauch, arXiv:1207.6108 [hep-ph]; A. Djouadi, arXiv:1208.3436 [hep-ph]; B. Batell, S. Gori and L. T. Wang, arXiv:1209.6832 [hep-ph].

- [5] T. Aaltonen *et al.* [CDF and D0 Collaborations], arXiv:1207.6436 [hep-ex]; see also TEVNP Working Group, for the CDF and D0 Collaborations arXiv:1207.0449 [hep-ex].
- [6] J. Ellis, D. S. Hwang, V. Sanz and T. You, arXiv:1208.6002 [hep-ph].
- [7] See, for example S. Y. Choi, D. J. . Miller, M. M. Muhlleitner and P. M. Zerwas, Phys. Lett. B **553** (2003) 61 [arXiv:hep-ph/0210077]; K. Odagiri, JHEP **0303** (2003) 009 [arXiv:hep-ph/0212215]; C. P. Buszello, I. Fleck, P. Marquard and J. J. van der Bij, Eur. Phys. J. C **32** (2004) 209 [arXiv:hep-ph/0212396]; A. Djouadi, Phys. Rept. **457** (2008) 1 [arXiv:hep-ph/0503172]; C. P. Buszello and P. Marquard, arXiv:hep-ph/0603209; A. Bredenstein, A. Denner, S. Dittmaier and M. M. Weber, Phys. Rev. D **74** (2006) 013004 [arXiv:hep-ph/0604011]; P. S. Bhupal Dev, A. Djouadi, R. M. Godbole, M. M. Muhlleitner and S. D. Rindani, Phys. Rev. Lett. **100** (2008) 051801 [arXiv:0707.2878 [hep-ph]]; R. M. Godbole, D. J. . Miller and M. M. Muhlleitner, JHEP **0712** (2007) 031 [arXiv:0708.0458 [hep-ph]]; K. Hagiwara, Q. Li and K. Mawatari, JHEP **0907** (2009) 101 [arXiv:0905.4314 [hep-ph]]; A. De Rujula, J. Lykken, M. Pierini, C. Rogan and M. Spiropulu, Phys. Rev. D **82** (2010) 013003 [arXiv:1001.5300 [hep-ph]]; C. Englert, C. Hackstein and M. Spannowsky, Phys. Rev. D **82** (2010) 114024 [arXiv:1010.0676 [hep-ph]]; U. De Sanctis, M. Fabbrichesi and A. Tonerio, Phys. Rev. D **84** (2011) 015013 [arXiv:1103.1973 [hep-ph]]; V. Barger and P. Huang, Phys. Rev. D **84** (2011) 093001 [arXiv:1107.4131 [hep-ph]]; S. Bolognesi, Y. Gao, A. V. Gritsan, K. Melnikov, M. Schulze, N. V. Tran and A. Whitbeck, arXiv:1208.4018 [hep-ph]; R. Boughezal, T. J. LeCompte and F. Petriello, arXiv:1208.4311 [hep-ph]; D. Stolarski and R. Vega-Morales, arXiv:1208.4840 [hep-ph]; S. Y. Choi, M. M. Muhlleitner and P. M. Zerwas, arXiv:1209.5268 [hep-ph].
- [8] R. Fok, C. Guimaraes, R. Lewis and V. Sanz, arXiv:1203.2917 [hep-ph].
- [9] T. Gherghetta and A. Pomarol, Nucl. Phys. B **586**, 141 (2000) [hep-ph/0003129].
T. Gherghetta and A. Pomarol, Nucl. Phys. B **602**, 3 (2001) [hep-ph/0012378].
- [10] L. Randall, V. Sanz and M. D. Schwartz, JHEP **0206**, 008 (2002) [hep-th/0204038].
- [11] J. Hirn and V. Sanz, Phys. Rev. D **76**, 044022 (2007) [hep-ph/0702005 [HEP-PH]].
Phys. Rev. Lett. **97**, 121803 (2006) [hep-ph/0606086]. JHEP **0703**, 100 (2007) [hep-ph/0612239].

- [12] S. Eidelman *et al.* [Particle Data Group Collaboration], Phys. Lett. B **592**, 1 (2004).
- [13] A. L. Fitzpatrick, J. Kaplan, L. Randall and L. -T. Wang, JHEP **0709**, 013 (2007) [hep-ph/0701150].
- [14] Y. Grossman and M. Neubert, Phys. Lett. B **474**, 361 (2000) [hep-ph/9912408].
- [15] Y. Gao, A. V. Gritsan, Z. Guo, K. Melnikov, M. Schulze and N. V. Tran, Phys. Rev. D **81** (2010) 075022 [arXiv:1001.3396 [hep-ph]].
- [16] J. Ellis and D. S. Hwang, JHEP **1209** (2012) 071 [arXiv:1202.6660 [hep-ph]].
- [17] J. Alwall *et al.*, *MadGraph 5 : Going Beyond*, JHEP **1106**, 128 (2011) [arXiv:1106.0522 [hep-ph]].
- [18] T. Sjostrand, S. Mrenna and P. Z. Skands, *PYTHIA 6.4 Physics and Manual*, JHEP **0605**, 026 (2006) [hep-ph/0603175].
- [19] S. Ovin, X. Rouby and V. Lemaitre, *Delphes, a framework for fast simulation of a generic collider experiment*, arXiv:0903.2225 [hep-ph].
- [20] A. Alves, arXiv:1209.1037 [hep-ph].
- [21] R. Cousins, J. Mumford, J. Tucker, and V. Valuev, JHEP **11** (2005) 046.
- [22] N. D. Christensen and C. Duhr, *FeynRules - Feynman rules made easy*, Comput. Phys. Commun. **180** (2009) 1614 [arXiv:0806.4194 [hep-ph]].
- [23] C. Degrande, C. Duhr, B. Fuks, D. Grellscheid, O. Mattelaer and T. Reiter, *UFO - The Universal FeynRules Output*, Comput. Phys. Commun. **183** (2012) 1201 [arXiv:1108.2040 [hep-ph]].
- [24] ATLAS Collaboration,
<https://atlas.web.cern.ch/Atlas/GROUPS/PHYSICS/CONFNOTES/ATLAS-CONF-2012-127/>.